Applied Physics Letters

PERSPECTIVE | FEBRUARY 12 2024

Perspectives on phononic waveguides for on-chip classical and quantum transduction

Yanan Wang ; Jaesung Lee ; Philip X.-L. Feng

Appl. Phys. Lett. 124, 070502 (2024)
https://doi.org/10.1063/5.0176867

AIP Publishing

Applied Physics Letters PERSPECTIVE pubs.aip.org/aip/apl

Perspectives on phononic waveguides for on-chip classical and quantum transduction

Cite as: Appl. Phys. Lett. **124**, 070502 (2024); doi: 10.1063/5.0176867
Submitted: 18 September 2023 · Accepted: 10 January 2024 ·
Published Online: 12 February 2024

Yanan Wang,[1,a] Jaesung Lee,[2,a] and Philip X.-L. Feng[3,a]

AFFILIATIONS

[1]Department of Electrical and Computer Engineering, College of Engineering, University of Nebraska, Lincoln, Nebraska 68588, USA
[2]Department of Electrical and Computer Engineering, College of Engineering, University of Central Florida, Orlando, Florida 32816, USA
[3]Department of Electrical and Computer Engineering, Herbert Wertheim College of Engineering, University of Florida, Gainesville, Florida 32611, USA

[a]**Authors to whom correspondence should be addressed:** yanan.wang@unl.edu; jaesung.lee@ucf.edu; and philip.feng@ufl.edu

ABSTRACT

Phononic waveguides (PnWGs) are devices with rationally designed periodic structures to manipulate mechanical oscillations and to engineer and control the propagation of acoustic waves, thus allowing for frequency and band selection of wave transmission and routing, promising for both classical and quantum transduction on chip-scale platforms with various constituent materials of interest. They can be incorporated into both electromechanical and optomechanical signal transduction schemes. Here, we present an overview of emerging micro/nanoscale PnWGs and offer perspectives for future. We evaluate the typical structural designs, frequency scaling, and phononic band structures of the PnWGs. Material choices, fabrication techniques, and characterization schemes are discussed based on different PnWG designs. For classical transduction schemes, an all-phononic integrated circuit perspective is proposed. Toward emerging quantum applications, the potential of utilizing PnWGs as universal interfaces and transduction channels has been examined. We envision PnWGs with extraordinary propagation properties, such as nonreciprocity and active tunability, can be realized with unconventional design strategies (*e.g.*, inverse design) and advanced materials (*e.g.*, van der Waals layered crystals), opening opportunities in both classical and quantum signal transduction schemes.

INTRODUCTION

Phonons, quanta of acoustic waves and mechanical vibrations,[1,2] are ubiquitous for signal processing and communication. For example, human verbal communications are via acoustic waves at audible frequencies; wireless communication devices greatly exploit radio frequency (RF) and microwave mechanical oscillations and waves in piezoelectric crystals for timing and signal processing. Phononics generally refers to studies of acoustic and vibrational waves over a much broader spectrum [Fig. 1(a)], ranging from infrasounds (< 20 Hz), audible sound (20 Hz–20 kHz), ultrasounds (20 kHz–1 GHz), and hypersounds (1 GHz–1 THz), to lattice vibrations (heat at room temperature, $\gtrapprox$ 1 THz). Phonons at these frequency bands play essential roles as information and energy carriers and have empowered numerous applications from infrasonic earthquake detection,[3] sonic navigation and ranging (sonar),[4] noise mitigation,[5] ultrasound imaging,[6] to thermal management.[7]

The routing of acoustic waves can be implemented with phononic waveguides (PnWGs) based on boundary confinement or the spatial distribution and modulation of the material constants in the structures. The former approach utilizes the phase or impedance mismatch between different media, analogous to optic fibers,[8] and ridge and slab photonic waveguides.[9,10] As exemplified in the cladding/core/cladding structure [Fig. 1(b)], the acoustic wave, as a scalar wave, will be confined within the homogeneous core with a relatively low velocity of waves compared to that in the cladding regions. The latter approach has been successfully realized in artificial structures, such as phononic crystals (PnCs) and acoustic metastructures. Similar to photonic crystals (PhCs), periodic geometrical or elastic structures in PnCs that mimic the arrangement of atoms in natural crystals yield phononic band structures [Fig. 1(c)]. The appearance of the second-order Brillouin zones and consequential zone folding gives rise to the modification of phonon dispersion and the complex band features (*e.g.*, passbands, stopbands, and bandgaps) for guided waves.

Beyond the guiding mechanisms, the working frequency/wavelength is one of the primary parameters to be considered. In general, the confinement of waveguides rises from interference effects; hence, the

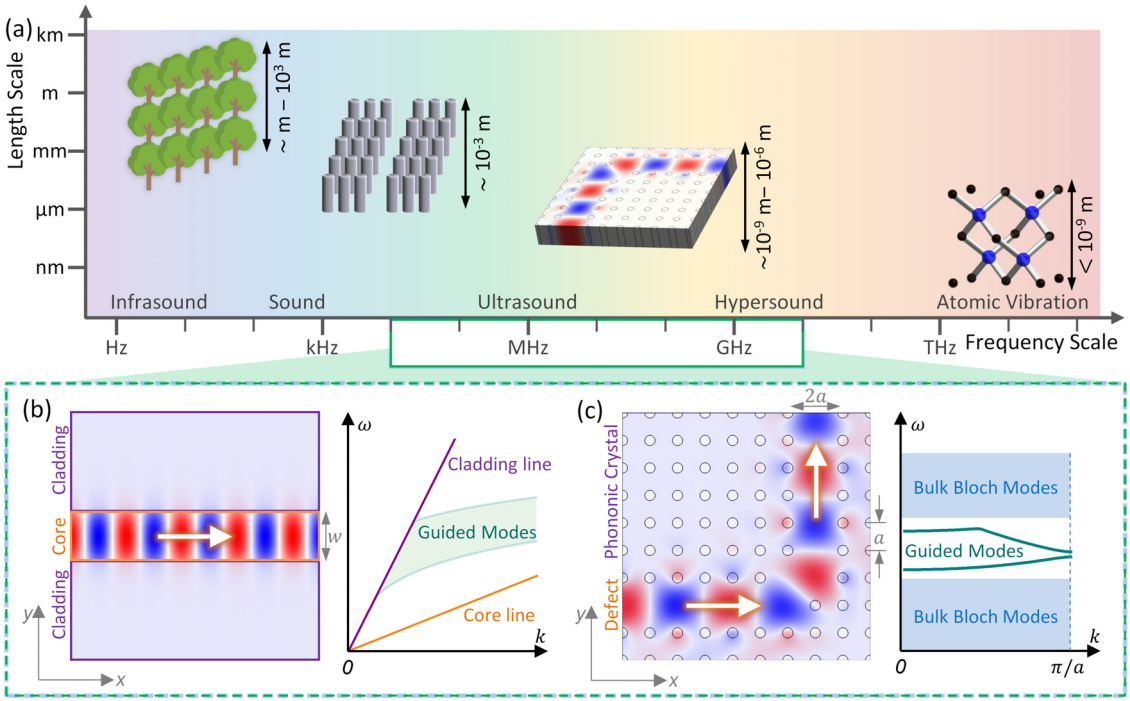

FIG. 1. Overview of phononic waveguides (PnWGs). (a) The phononic spectrum with size (characteristic length, such as waveguide width *w* and phononic lattice period *a*) dependency and frequency scaling for the typical corresponding structures and devices. The mechanisms of phononic waveguiding are based on (b) boundary confinement in a homogenous structure and (c) spatial distribution and modulation of the material constants in a periodic structure. The dispersion plots exhibit the relation between angular frequency ω and wavenumber k.

phonon wavelengths λ are comparable to the phononic structures. Figure 1(a) illustrates such frequency scaling of phononic devices: infrasound and sound frequencies are usually associated with macroscale objects, while for ultrasound and high-frequency operations, micro/nanostructured devices are required. Following the frequency scaling, this Perspective article focuses on phononic waveguides that operate at radio to microwave frequencies (20 kHz–300 GHz) and their applications toward on-chip signal conversion and transmission, also referred to as modalities of transduction, in both classical and quantum regimes. The design strategies (*e.g.*, quasi-one-dimensional coupled resonator array, linear defects in two-dimensional phononic crystals, and topological structures) and corresponding metrics (*e.g.*, degree of confinement and transmittance, working frequency and bandwidth, and the dispersion relation for guided waves) will be discussed in section "Design Strategies and Mechanisms." Material choices, measurement, and characterization schemes will be introduced in section "Implementation and Characterization." The state-of-the-art and emerging applications in classical and quantum domains will be reviewed and examined in sections "Applications in Classical Signal Processing" and "Applications Toward Quantum Transduction," respectively.

DESIGN STRATEGIES AND MECHANISMS

Homogeneous structures

One of the simplest geometries that support acoustic wave transmission is a one-dimensional (1D) homogeneous beam with continuous translational symmetry. In the loss-less 1D structure, the acoustic signal propagates with a relation of $\partial^2 u/\partial t^2 = c^2 \partial^2 u/\partial x^2$, where u is the displacement, t is the time, x is the location on the beam, and c is the speed of sound in the material, and thus, it can be transmitted as time-dependent longitudinal and also transverse waves.

The acoustic waves are characterized by the wavenumber k and phase velocity v; and their interactions with media, such as reflection and refraction, obey Fermat's principle and Snell's law in the classic domain.[11,12] Hence, wave confinement and guiding can be implemented with a cladding/core/cladding structure, as depicted in Fig. 1(b), based on the contrasting speeds of sound ($c = v = \sqrt{E_{\text{Bulk}}/\rho}$, where v is the phase velocity of the acoustic wave, E_{Bulk} is the bulk modulus, and ρ is the mass density) and phase mismatch in different media. Total internal reflection occurs if the acoustic wave in the core is not phase-matched with any leaky/evanescent modes in the cladding. To achieve such a condition and confine the acoustic wave inside the homogeneous core, the speed of sound and phase velocity in the core must be slower than the ones in the cladding ($v_{\text{core}} < v_{\text{cladding}}$).[13,14] The phase velocity can be represented as the slope in the dispersion diagram, which describes the relationship between the angular frequency ω as a function of the wavenumber k, $v = d\omega/dk$. As shown in the right panel of Fig. 1(b), the bottom and top wave lines correspond to the dispersion relations for the core and the cladding, respectively; the dispersion relation for guided waves must appear in the cone delimited by these two wave lines. Furthermore, the guided modes in a PnWG can be described as approximate solutions of the Helmholtz equations. At a given frequency, a waveguide has only a finite number of guided propagation modes, of which transverse amplitude profiles and propagation constants depend on the

design of the waveguide structure. Monomodal propagation can be facilitated when the core size is comparable to the wavelength ($\lambda = 2\pi/k$).

The cladding/core/cladding structures discussed above are analogous to the optical fibers and photonic waveguides, in which both acoustic and electromagnetic waves are confined in slower media due to total internal reflection,[8–10,13,14] while some distinctive properties of acoustic waves need to be taken into consideration as well. In some configurations, even though total internal reflection cannot be satisfied ($v_{core} > v_{cladding}$), strong reflection and phononic confinement can still be realized at interfaces between media with widely different acoustic impedances ($\eta = c \cdot \rho$), such as between solids and gases. The speed of sound in air is generally lower than the values in solid structural materials;[15–31] however, the solid–air boundary geometrically softens the structural response of the material and, thus, lowers the effective phase velocity.[11,32] In such a scenario, instead of phonon confinement inside the bulk media, slow surface acoustic waves (SAWs) are generated and constrained to the interfaces.[33–35] Surface acoustic waves permit more flexibility in material choice and geometric design.[34–40] Such as topographic waveguides consisting of local deformation of the substrate surface itself can be utilized.

Quasi-1D coupled resonator array

Coupling individual resonators into quasi-one-dimensional (quasi-1D) arrays offers more flexibility to control the acoustic wave propagation beyond the homogeneous structures. By engineering the geometry of resonators, the coupling strength between the resonators, and the periodicity of the array, the dispersion relations can be finely tuned; thus, frequency-dependent passing and stopping of the wave propagation can be achieved.

A representative design is a coupled block array that mimics a 1D diatomic chain typically studied in solid-state physics [Fig. 2(a)].[41] For a 1D diatomic chain consisting of alternating small and large masses coupled by springs, the two masses moving in-phase in each unit cell give rise to low-frequency acoustic phonon modes, while the two masses moving out-of-phase engender higher frequency optical phonon modes. The frequency bandgap between low and high frequency vibrations becomes more pronounced with increasing difference in these particle masses. For a quasi-1D block array consisting of a linear array of blocks joined together by narrower connecting links, the wave velocities and the dispersion can be more accurately described by an effective medium theory and a tight-binding model in the low and high frequencies, respectively.[42–44] In order to produce a sizable bandgap, which is useful for constructing wavelength-selective devices and RF filters, the effective medium bands can be squeezed down to lower frequencies by reducing the width of the couplers. The consequential reduction of coupling strength between the blocks also flattens the slope of the tight-binding bands, complementing each other to increase the phononic bandgap. Following such a design principle, Fig. 2(a) exemplifies a quasi-1D array of rigid silicon (Si) sub-micron-sized blocks

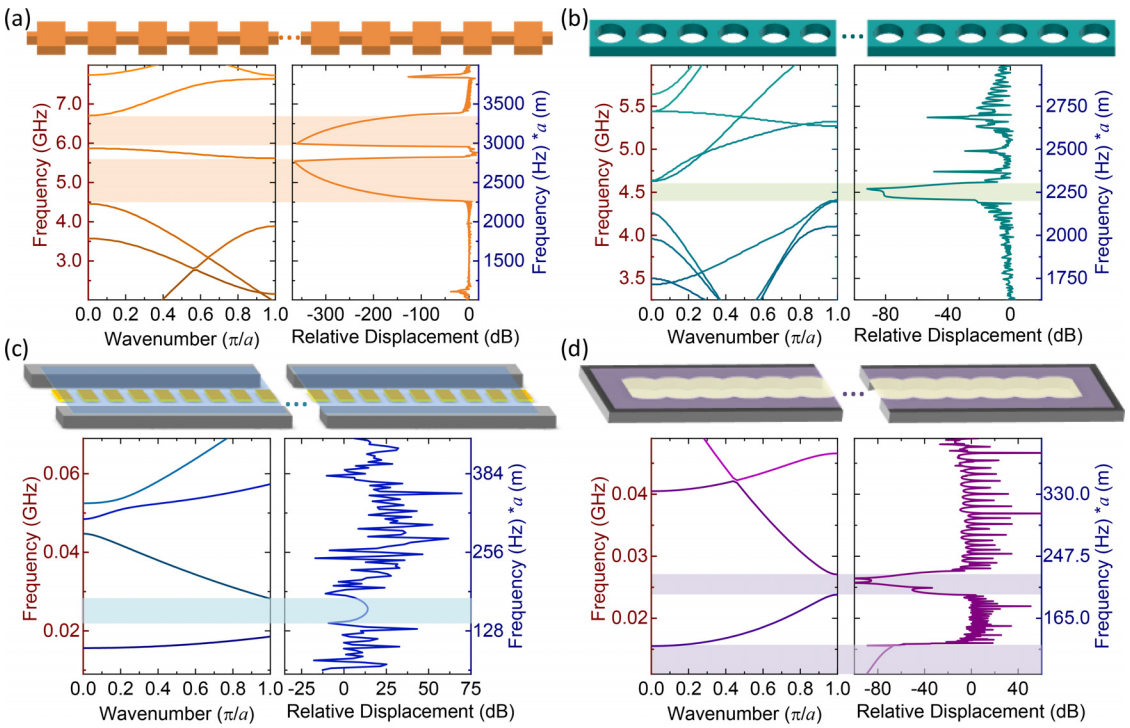

FIG. 2. Quasi-1D phononic crystal lattices based on the periodic geometric conditions of (a) block array (array period $a = 500$ nm, square block size $b = 400$ nm, link width $w_L = 100$ nm, and thickness $h = 250$ nm) and (b) air-hole array (array period $a = 500$ nm, beam width $w_B = 500$ nm, hole diameter $d = 450$ nm, and thickness $h = 100$ nm), (c) periodic elastic conditions (array period $a = 18\ \mu$m, trench width $w_T = 12\ \mu$m, thickness $h = 120$ nm, and tension ratio $T_{max}/T_{min} = 100$), and (d) a hybrid scheme (array period $a = 9\ \mu$m, unit cell width $w_U = 12\ \mu$m, and thickness $h = 120$ nm). The block array and air-hole structures are based on silicon (Si) with Young's modulus of 170 GPa and mass density of 2329 kg/m^3. The elastic and hybrid schemes are based on two-dimensional (2D) materials with Young's modulus of 370 GPa and mass density of 2100 kg/m^3.

(block width × length = 400 × 400 nm^2) connected through short links (link width × length = 100 × 100 nm^2), which allows a narrow phononic passing band (~5.6–5.9 GHz) sandwiched between the first and second bandgaps. Moreover, because the frequency response is inversely proportional to the size of the device [right axis in Fig. 2(a)], simply increasing or decreasing the dimensions of the unit cell (block size, link width, and thickness, proportionally) can tune the narrow passing band over the most acoustic spectrum of interest.

The alternating masses can also be achieved by utilizing a beam with periodic air holes [Fig. 2(b)]. The circular hole geometry possesses high symmetry and simplicity in fabrication; however, this design is more efficient for the beams with considerable width-to-thickness ratios (w_B/h), which work in the tension-dominated membrane region. For rigid beams in Young's modulus-dominated region, complete phononic bandgaps can only be observed when the ratio between the hole diameter and the beam width d/w_B is large enough for a narrow range of beam thickness. For instance, the phononic bandgap around 4.5 GHz that is observed for a 100 nm thick Si nanobeam with a period of 500 nm, beam width of 500 nm, and air-hole diameter of 450 nm ($d/w_B = 0.9$) will vanish when the thickness increases to 125 nm or decreases to 75 nm. Hence, oval-shaped holes or rectangular slots with less symmetry are more commonly adopted in practical designs for rigid beams.[44–50]

Instead of alternating the masses, PnWG can also be implemented with alternative elastic properties. Figures 2(c) and 2(d) exemplify elastically modulated quasi-1D waveguides based on two-dimensional (2D) materials. Thanks to the high Young's modulus, low rigidity, and low mass,[51–53] strain engineering and consequential tuning of mechanical resonances have been successfully demonstrated in 2D materials, such as graphene, transition metal dichalcogenides (TMDCs), and 2D materials heterostructures, by employing modest electrostatic forces.[53–55] Taking the design in Fig. 2(c) as an example, the application of DC voltage to the gate electrode array underneath a suspended graphene waveguide exerts an electrostatic force on the graphene, which induces stretching toward the electrodes.[56] This electrostatic stretching forms a periodic elastic potential in the PnWG and modulates the dispersion relation of traveling acoustic waves, providing a noninvasive approach to opening the phononic bandgaps. Moreover, alternating the DC voltage applied to the electrode array can realize dynamic control over the propagation properties of the PnWG,[57,58] such as a transition from transparency to opacity and trapping of the acoustic waves in an arbitrary position, and empower active phononic components (with amplification gain) for the integrated circuits. Figure 2(d) presents a hybrid scheme based on both alternating masses and elastic constraints in a suspended hexagonal boron nitride (h-BN) waveguide.[59] Such a waveguide consists of circular drumhead resonators overlaying with each other and forming quasi-oval-shaped unit cells. The alternating supported and suspended areas result in periodic elastic conditions. The coupling strength and phononic band structure can be effectively tuned by controlling the overlaying area between the adjacent drumheads. It is worth noting that the alternative elastic and hybrid approaches are also applicable to conventional thin films, such as silicon nitride (SiN_x) and aluminum gallium arsenide (AlGaAs).[60–63] Moreover, frequency scaling can be easily achieved by varying the size of the unit cells in all the aforementioned quasi-1D array designs, following the relation plotted as the right axes of Fig. 2.

Linear defect in 2D phononic crystal

2D phononic crystals (PnCs) can be constructed by simply extending the quasi-1D array discussed above. For instance, the PnC shown in Fig. 3 shares elements of square blocks and thin connectors similar to the quasi-1D array shown in Fig. 2(a) but is now arranged in two dimensions. The phononic band structure, including all symmetries of vibrational modes, is plotted along the high symmetry points of the first Brillouin zone in a 2D square lattice [Fig. 3(a)]. Analogous to the atomic lattices in natural crystals, the appearance of second-order Brillouin zones leads to the modification of the phonon dispersion and zone folding. Complex features, such as bandgaps due to Bragg reflections or band hybridization of periodic scatters, emerge.[64–66]

Distinguishing from the quasi-1D arrays discussed above, in which the acoustic waves are inherently confined and propagate along the waveguide directions, the acoustic waves can propagate along arbitrary in-plane directions in 2D PnCs. Hence, to create effective 1D confinement in 2D structures, a concept of defect state is borrowed from solid-state physics. It is well known that introducing defects

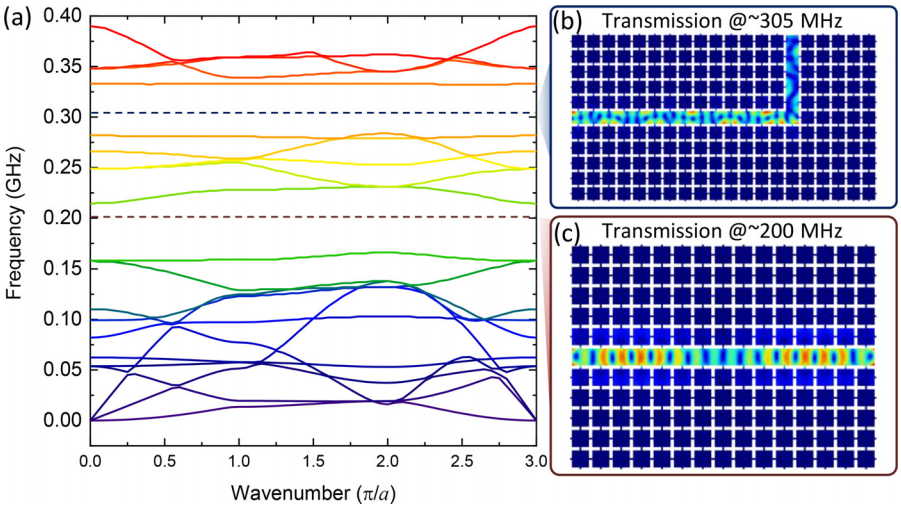

FIG. 3. Linear defects in 2D phononic crystal with block-chain unit cells. (a) Phononic dispersion plot of a 2D PnC (array period $a = 12\ \mu$m, square block size $b = 10\ \mu$m, link width $w_L = 1\ \mu$m, and thickness $h = 1\ \mu$m) with Floquet periodicity. Transmission of linear defect phonon modes at frequencies of (b) ~200 and (c) ~305 MHz, labeled as wine and navy dashed lines in the dispersion plot, respectively. The 2D PnC is simulated based on Si with Young's modulus of 170 GPa and mass density of 2329 kg/m^3.

inside an otherwise perfectly atomic lattice will give rise to the localized defect states and the conduction of electrons within the bandgap. Similarly, defect modes can be realized in PnC lattices as well, providing additional degrees of freedom to manipulate the acoustic wave propagation. The phononic waveguide can be created by introducing a whole row of defects in a 2D PnC.[67–70] Such a phononic crystal waveguide can be pictured as a homogeneous core sandwiched between two sets of 2D PnCs. For waves to be confined and guided, their frequencies must fall within the bandgap of the PnCs. Once a guided mode is excited inside the core, it will propagate with little perturbation because the eigenmodes of the crystals are translationally invariant. A more analytical and accurate description can be provided by the supercell model,[71,72] in which the number of periods of the 2D PnC is reduced by one, and the superlattice is still periodic along its principal axis. Consequently, highly dispersive and interfering bands, as guided bands, appear within the bulk bandgap of the original 2D PnC. Periodicity of the supercell implies that band folding and bandgap opening also occur for the guided bands. Apparently, the operation bandwidth of such a phononic crystal waveguide cannot exceed the bandgap width of the bulk crystal. Hence, for broadband operations, wide bandgaps are favorable. On the other hand, by engineering the bandgaps and the defect modes, single-mode operation at a desired frequency can be facilitated in such defect-mode waveguides, which is hard to achieve in homogeneous and quasi-1D array designs.

Moreover, bent waveguides can be realized by engineering the defects in 2D PnCs [Fig. 3(c)]. It is worth mentioning that abrupt bends between straight waveguides may induce significant scattering. Hence, modeling with scattering matrices,[73] which accounts for reflection and transmission between normal modes, is more suitable and practical for phononic circuit design.

Topological structures

Inspired by topological insulators in condensed matter physics, a class of materials that possess unique electronic conduction properties, topological structures have been proposed and explored in the phononic domain.[74–78] As suggested by the name, topological insulators are characterized by a sizeable bandgap and are electronically nonconductive in their bulk. However, the topological features of the valence and conduction bands lead to the emergence of edge states for such materials with finite sizes. For instance, in the theory of the quantum Hall effect,[79,80] a 2D electron gas is placed in an out-of-plane uniform magnetic field, which breaks the time-reversal symmetry of the system. This leads to the electrons only orbiting in one direction and the consequential cyclotron orbits being quantized to discrete levels, known as the Landau levels. When the system is finite, the break of cyclotron orbits at the edges forces the electrons to jump to the next orbit and form a one-way current flow. It is noticed that such a current exists independent of the boundary shape or the presence of continuous defects and imperfections as long as those do not affect the bandgap topology. The unidirectional propagation without backscattering and unusual robustness to defects and disorder make topological insulators valuable material platforms for waveguiding.

Based on the above-mentioned discussion in condensed matter physics, it is clear that electron spin plays a fundamental role in defining the topological edge states. Given that sound does not possess an intrinsic spin, the key to realizing topological structures in the phononic domain is to create acoustic pseudospins. Angular momentum,[81] geometrical asymmetries,[82,83] structured space- and time-dependent material properties,[84,85] and asymmetric nonlinearities[86] have been explored as pseudospins experimentally.

IMPLEMENTATION AND CHARACTERIZATION

Material choices

It is worth mentioning that the PnWG design schemes exemplified in section "Design Strategies and Mechanisms" are general and universal. Meanwhile, fundamental material properties, such as Young's modulus, mass density, breaking limit, piezoelectric coefficient, and electron conductivity, still need to be considered in practical

TABLE I. Mechanical and related properties of the typical structural materials for on-chip PnWG. Mass density: ρ (kg/m^3), Young's modulus: E_Y (GPa), speed of sound: c (m/s), acoustic impedance: Z (10^6 kg/m^2/s), thermal conductivity: κ (W/m/K), Debye temperature: Θ_D (K), piezoelectric coefficient: d (pm/V), and Akhiezer-limited frequency and quality factor product: $f \times Q$ (THz).

Materials	ρ (kg/m^3)	E_Y (GPa)	c (m/s)	Z (10^6 kg/m^2/s)	κ (W/m/K)	Θ_D (K)	d (pm/V)	$f \times Q$ (THz)	Refs.
Si	2330	170	8433	20	140	645	N/A	23	16 and 17
SiO_2	2200 − 2650	75	5640	15	1.3	470	$d_{33} = 2.33$	32	16, 18, and 19
SiN_x	3170	270	9000	30	20	1750	N/A	130	20
AlN	3300	300 − 350	10 170	34	290	1150	$d_{31} = -2.6$ $d_{33} = 5.5$	25	18 and 21–23
GaN	6150	320	7300	25	130	600	$d_{31} = -1.7$ $d_{33} = 3.4$	30	21 and 22
$LiNbO_3$	4630	203	3990	34	5.6	307	$d_{15} = 69$	230	19, 21, 24, and 25
Diamond	3510	1054	12 000	42	600 − 1000	2340	N/A	37	16 and 26
SiC	3210	430	9500	31	500	1200	N/A	640	21
Graphene	2267	1000	21 800	47	2500	1813	N/A	37	27 and 28
h-BN	2100	870	20 300	42	450	1900	$d_{11} = 0.61$	62	16, 27, and 29
MoS_2	5060	300	7700	39	68	262.3	$d_{11} = 3.65$	180	30 and 31
Air	1.2	1.4×10^{-4}	346	413	0.026	N/A	N/A	N/A	15, 16, and 19

implementations. Table I summarizes the key metrics of conventional and emerging structural materials for micro/nanoelectromechanical systems (MEMS/NEMS). As discussed in the homogeneous design, phononic confinement is not easily achievable in silicon-on-insulator (SOI), the canonical platform of integrated electronics and photonics because the acoustic waves preferably propagate in the silicon dioxide (SiO_2) cladding with a lower speed of sound rather than the silicon (Si) core. For SAW guiding, materials that exhibit relatively large piezoelectric coefficients, such as aluminum nitride (AlN), gallium nitride (GaN), and lithium niobate ($LiNbO_3$), are favorable.[21] Also, as mentioned in the quasi-1D coupled resonator array design, thin films and 2D materials with large aspect ratios between lateral dimensions and layer thicknesses are advantageous for realizing the period elastic schemes.

In real applications, loss and transmission speed are critical metrics as well. For PnWGs composed of homogeneous materials, the fundamental upper limit of signal transmission distance is determined by an energy loss mechanism associated with phonon–phonon damping in the material, known as the Akhiezer effect.[87,88] The Akhiezer effect is particularly significant when other acoustic loss mechanisms (such as clamping loss and thermoelastic damping) are suppressed, and the devices are operating at relatively low frequencies ($\omega\tau < 1$, typically $f < 1-10$ GHz, where τ represents the phonon thermal relaxation time). The Akhiezer limit of quality factor (Q) can be calculated by $Q = \frac{\rho c^4}{2\pi\eta^2\kappa T f}$, where ρ is the mass density, c is the averaged acoustic velocity, η is the average Grüneisen's parameter, κ is the thermal conductivity, T is the temperature, and f is the operating frequency of devices. The Akhiezer limit is often described in the form of $f \times Q$, and materials such as silicon carbide (SiC) and silicon nitride (SiN_x) exhibit relatively high Akhiezer-limited $f \times Q$ (shown in Table I). Additionally, materials (such as SiC, diamond, graphene, and h-BN) exhibiting high speed of sound $c = \sqrt{\frac{E_{\text{Bulk}}}{\rho}}$ is desirable for high-frequency and high-speed applications.

Here, we shall highlight the unique combination of large modulus and low mass density of 2D materials endorsing promising applications in high frequency regimes.[51–55] In addition, high breaking limits make them suitable platforms for strain tuning and dynamic control of PnWG performance. Figure 4 shows simulated phonon dispersion in the graphene PnWG that has a square unit cell with an air hole. We find that by changing the strain level of the PnWG, the frequency responses of the device are greatly modified, giving highly tunable band features. Thanks to the ultrahigh strain limit of 2D crystals ($\varepsilon_{\text{limit}} \sim 25\%$ for graphene),[51] they could offer a much broader tuning range for PnWG that cannot be easily achievable in conventional 3D materials such as Si with much lower strain limits.

Device fabrication and characterization schemes

Phononic waveguides based on SAW can be fabricated by using a piezoelectric layer-on-substrate wafer, such as $LiNbO_3$-on-sapphire or GaN-on-Si.[89–93] The waveguide pattern is transferred using either photo- or electron beam lithography. Subsequently, the exposed piezoelectric layer is removed using dry etching methods. Once the waveguide structure is defined in the piezoelectric layer, the interdigital transducer (IDT) metallization layer is patterned through lithography, followed by metal deposition and a liftoff process. To characterize the SAW phononic waveguides, a microwave signal is applied as an input to the first IDT, which excites mechanical wave through piezoelectric coupling [Fig. 5(a)]. Once the propagating wave reaches the second IDT, the wave can be reflected, scattered, dissipated to the substrate, or converted back to an electrical signal, allowing us to measure transmission (S_{21}) through the IDT-waveguide-IDT system.

Suspended phononic waveguides can be fabricated by removing an underneath sacrificial layer after defining and patterning the device structure. Electrostatic actuation and readout can be performed through a parallel-plate capacitor between the waveguide and underneath electrodes [Fig. 5(b)]. By introducing both DC and RF voltages to the device and electrodes, electrostatic force excites mechanical vibrations that propagate through the waveguide. At the output port, a capacitive detection scheme is configured to sense mechanical vibration by measuring variation of capacitance between the device and electrodes. In addition to electrical characterization, mechanical wave propagation in the waveguides can be measured via a two-laser interferometry system [Fig. 5(c)],[59] where mechanical waves are

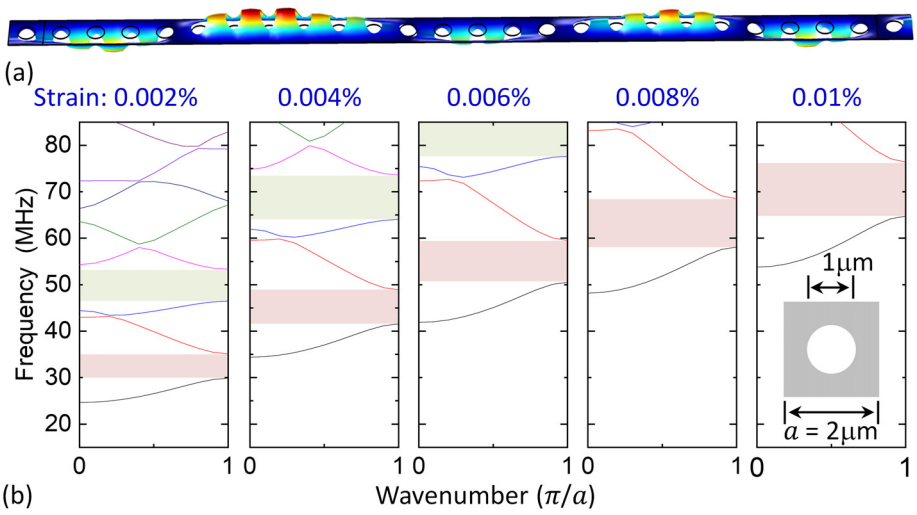

FIG. 4. Simulated single-layer graphene PnWG with different strain levels. (a) Simulated acoustic wave transmission. (b) Phonon dispersion curves with varying strain levels from 0.002% to 0.01%. Inset shows the structure and dimension of a phononic unit cell. Red and green colored areas represent the first and second phononic bandgaps, respectively.

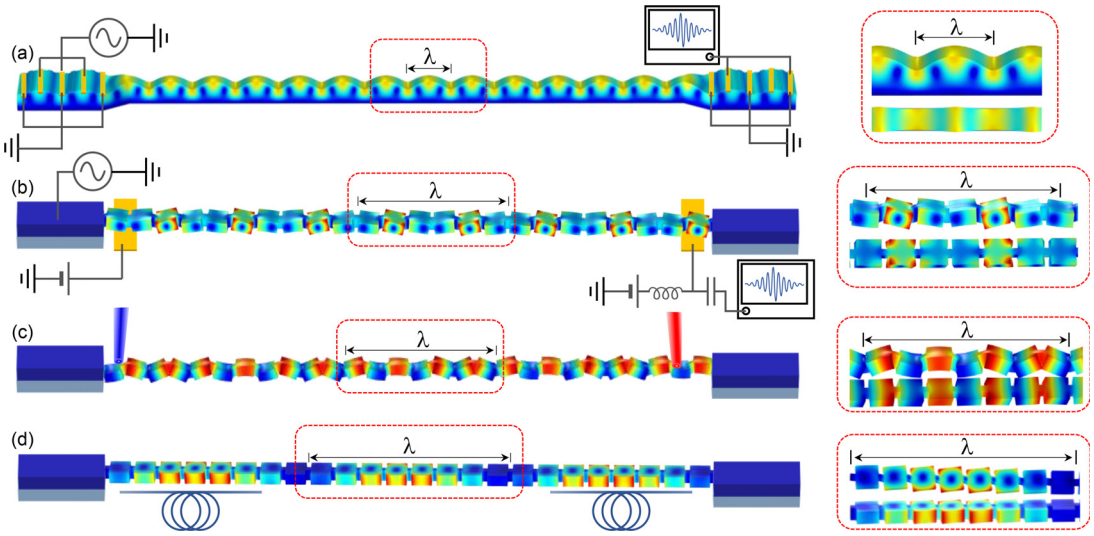

FIG. 5. Excitation and detection schemes for PnWG. (a) PnWG based on surface acoustic wave (SAW) structure with piezoelectric signal transduction. (b) Suspended PnWG and electrostatic acoustic wave excitation and detection scheme. (c) Two-laser drive-and-probe signal transduction in PnWG based on photothermal acoustic wave excitation (drive) and optical interferometry signal readout (probe). (d) PnWG with integrated photonics where the acoustic wave can be generated by radiation pressure and detected by optomechanical signal transduction.

photothermally excited using an amplitude-modulated laser and detected via continuous wave (CW) laser. Similarly, with strong optomechanical coupling enabled by introducing the device into a high Q optical cavity, radiation pressure can excite the mechanical vibration at the input transducer, and the traveling mechanical wave can be readout at the output port with optomechanical signal transduction [Fig. 5(d)].

APPLICATIONS IN CLASSICAL SIGNAL PROCESSING

Resonant MEMS have been widely employed for communications and signal processing applications thanks to their reducing size, weight, and power (SWaP) while retaining high Q factors. In such classical applications (*e.g.*, MEMS filters), signals should be translated from electrical to mechanical and then converted back to the electrical domain, leading to electromechanical coupling losses. To mitigate this issue, purely acoustic circuits in classical applications have been proposed, and some promising results have been reported.[89,94] Future all-acoustic RF front-end can be realized by connecting both passive and active mechanical components in the circuit using phononic waveguides, as shown in Fig. 6. Mechanical filters can be realized by engineering passbands and bandgaps in the phononic waveguides.[59–61] For example, a passband with the desired frequency can be sandwiched

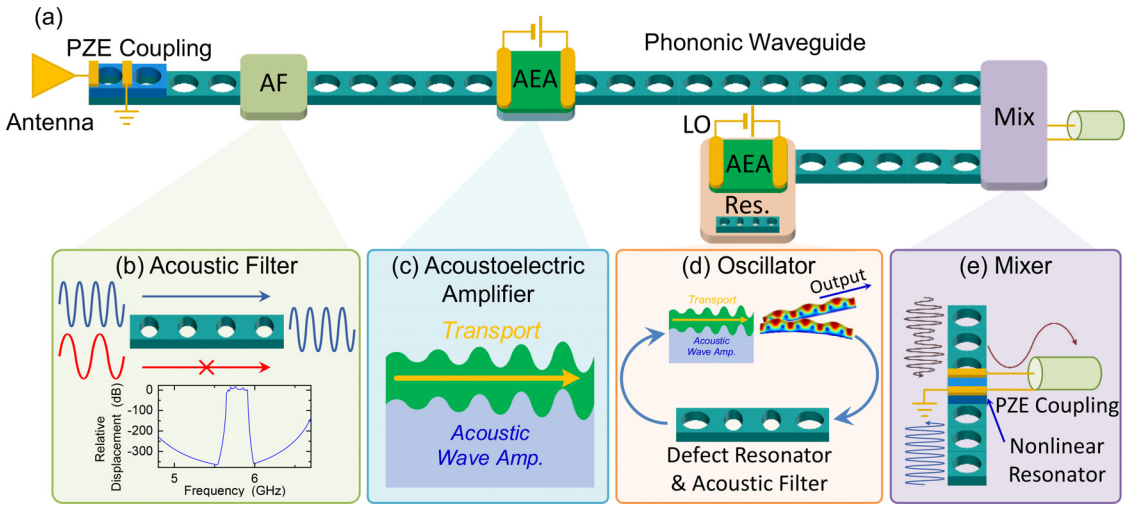

FIG. 6. Classical signal transduction via phononic waveguides in an all-mechanical circuit. (a) All-mechanical RF front-end that consists of (b) acoustic filter (AF) enabled by a transmission band sandwiched by two phononic bandgaps, (c) acoustoelectric amplifier (AEA), (d) acoustic local oscillator (LO), and (e) nonlinear acoustic mixer. The acoustic wave is excited through piezoelectric (PZE) coupling. Amp. stands for amplification, and Res. stands for resonator.

between the phononic bandgaps in the spectrum, which could enable a mechanical bandpass filter [Fig. 6(b)]. Similarly, high and low pass filters can be realized by adjusting the properties of pass/stopbands and bandgap. A voltage-controlled mechanical low noise amplifier (LNA) has been realized by using acoustoelectric (AE) interactions between the electronic charge carriers in the semiconductor and the electric fields. When electron and mechanical traveling waves hold similar propagation speeds, which enables strong AE effects leading to mechanical wave amplification or rejection. This AE effect has been demonstrated in various platforms (*e.g.*, GaN thin film bulk acoustic resonator,[90] AlN/Ge,[91] InGaAs/$LiNbO_3$,[89,92] and $LiNbO_3$/Si[93] SAW devices) with large AE terminal gain (~11.3 dB)[92] with continuous operations. A local oscillator (LO) can be realized by implementing a low-loss high Q mechanical resonator in phononic waveguides (*e.g.*, defect resonance within the phononic bandgap) and an AE amplifier (AEA) in the phononic circuit loop. By carefully designing mechanical wave round trip with control of loop gain, loss, and phase using the AE amplifier, Barkhausen criteria can be achieved for building a self-sustaining feedback phononic oscillator. In addition, passive components such as a mixer-filter combined device[93] can be developed by utilizing the mechanical nonlinearity of the phononic waveguide. Two different mechanical waves from RF and LO ports can be mixed in the waveguide through nonlinear frequency or amplitude signal mixing.[95]

It is worth noting that the employment of acoustic circuit components discussed above may still be limited in special practical applications. However, as we continue to advance the design of PnCs and PnWGs, and as the large-scale manufacturing techniques mature, the current barriers in cost-efficiency can be overcome. Accordingly, we envision that PnCs and PnWGs will play a significant role in future RF applications, especially in the spectrum range beyond super high frequency (SHF, 3 − 30 GHz).

APPLICATIONS TOWARD QUANTUM TRANSDUCTION

Unprecedented advances have been witnessed over the past decade in creating and controlling individual quantum entities in solid-state platforms, such as transmons using superconducting tunnel junctions,[96,97] spins in Si quantum dots,[98,99] and defect-related quantum emitters in wide-bandgap semiconductors.[100,101] An important and intriguing demand is to integrate quantum entities in such a way that the strengths of individual constituents can complement one another. For instance, superconducting transmons may be employed as computational quantum bits (qubits) due to fast processing speed, and solid-state spins may be exploited as quantum registers and memories for their long coherence times,[102,103] while photons may serve as flying qubits transmitted between remote quantum nodes.[104] Two crucial challenges in realizing hybrid architectures lie in the enormous energy/

TABLE II. Examples of phonon–qubit interactions and couplings. Phononic/acoustic devices utilized include high-overtone bulk acoustic resonators (HBARs), thin-film bulk acoustic resonators (FBARs), N/MEMS resonators, and mechanical cantilevers. Only solid-state quantum entities, including superconducting (SC) devices, quantum dots, and nitrogen vacancy (NV) centers in diamond, are listed here. The decoherence rates of qubits are calculated based on dephasing time $\gamma/2\pi = 1/2\pi T_2$ (Hz). The damping rates of the phononic/acoustic devices are calculated as $\zeta/2\pi = k_B T/(\hbar Q)$ (Hz), where k_B is the Boltzmann constant, T is the temperature, $\hbar$ is the reduced Planck constant, and Q is the quality factor.

	Coupling characteristics		Qubit characteristics		Phononic/acoustic characteristics		
Type of qubits	Phonon–qubit coupling mechanism	Coupling strength $g/2\pi$ (Hz) cooperativity $C = \frac{g^2}{\gamma\zeta}$	Frequency $\omega_q/2\pi$ (Hz)	Decoherence rate $\gamma/2\pi$ (Hz)	Frequency $\omega_c/2\pi$ (Hz)	Damping rate $\zeta/2\pi$ (Hz)]	References
SC devices	Capacitive coupling	2–120 MHz 0.04–490	6–10 GHz	20–50 MHz	60 MHz–6 GHz	0.1–500 MHz	105–107 and 110
	Lorentz force coupling	1 MHz $\ll 1$	~2 MHz	~1 MHz	~2 MHz	~180 kHz	108
	Piezoelectric coupling	260 kHz >260	6.684 GHz	27 kHz	6.678 GHz	9.4 kHz	109
Quantum dots	Strain coupling	140–450 kHz $\ll 1$	(Optical photons) ~336 and ~451 THz	1–10 GHz	500–800 kHz	80–220 MHz	112 and 113
	Piezoelectric coupling	(Theoretical) 10–450 MHz 11–55	(Charges) 725 GHz	(Charges) ~4 GHz (spins) ~0.5 MHz	(Theoretical) 1.5–6 GHz	(Theoretical) ~2.6 MHz	122
NV centers in diamond	Magnetic Coupling	< 100 Hz $\ll 1$	(Optical Photons) ~471 THz (Spin) 2.88 GHz	200 kHz–10 MHz	80 kHz–1 MHz	4–200 GHz	111
	Strain coupling	~3 kHz $\ll 1$	(Optical photons) ~471 THz (Spin) ~2.88 GHz	100 kHz–GHz	0.9–7 MHz	0.1–170 GHz	114–117
	Piezoelectric coupling	(Theoretical) 45–101 kHz 10–54	(Spin) ~2.88 GHz	(Theoretical) 10 Hz (at 20 mK)	(Theoretical) 3 GHz	(Theoretical) ~2.6 MHz	122

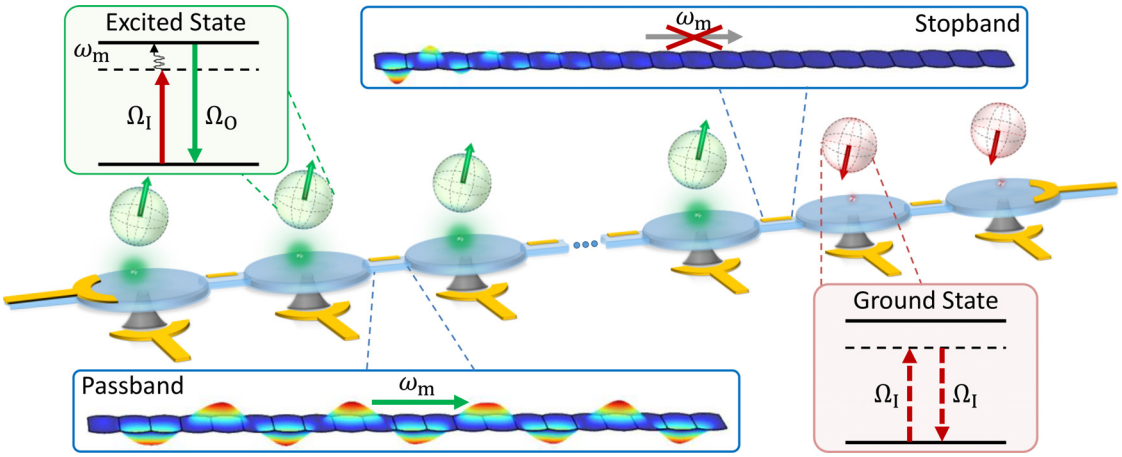

FIG. 7. Conceptual illustration of quantum emitters-embedded phonon network.

frequency discrepancy (from microwaves to visible light photons) and material incompatibility among the physical embodiments of these qubits. Hence, developing a universal bus interface that can efficiently and coherently mediate interactions and transduce quantum signals among various disparate physical components is the key to hybrid integration.

Phonons can provide distinctive pathways for coherent control of quantum states in various solid-state quantum entities. As exemplified in Table II, superconducting qubits can be coupled to phononic/mechanical devices via electrostatic or Lorentz force interactions.[105–110] In particular, the coherent energy exchange between superconducting qubits and microwave-frequency mechanical cavities has been experimentally demonstrated.[109,110] For solid-state spin qubits, crystal strain induced by the motion of phononic/mechanical devices can facilitate coupling to the orbital and spin degrees of freedom.[111–117] Quantum emitters-embedded phonon network has been proposed,[118] in which quantum states encoded in long-lived electronic spin states can be converted into propagating phonon wavepackets, transferred through a phononic waveguide, and then reabsorbed efficiently by a distant defect center (Fig. 7). In addition, optomechanical coupling can be readily realized via radiation-pressure force, enabling coherent signal transduction between photonic and phononic frequencies.[119]

Further encouraged by recent experimental demonstrations of phonon-mediated transduction between microwave and optical photons,[120,121] we envision phononic waveguides to be ideal interfaces for transducing quantum information among various quantum entities. The scheme of utilizing phonons as the universal bus is delineated in Fig. 8. Here, individual qubits (such as transmon qubits, spin qubits, and photon qubits) strongly interact with local cavities (such as microwave circuits, mechanical resonators, and optical cavities), which in turn can be coupled to a phononic waveguide. Each cavity-qubit coupled system can be considered as a quantum node and described using the generic Jaynes–Cummings Hamiltonian $H = \hbar\omega_c a^\dagger a + \hbar\omega_q \sigma_+\sigma_- + \hbar g\left(a^\dagger\sigma_- + a\sigma_+\right)$. The first term represents the energy of the cavity

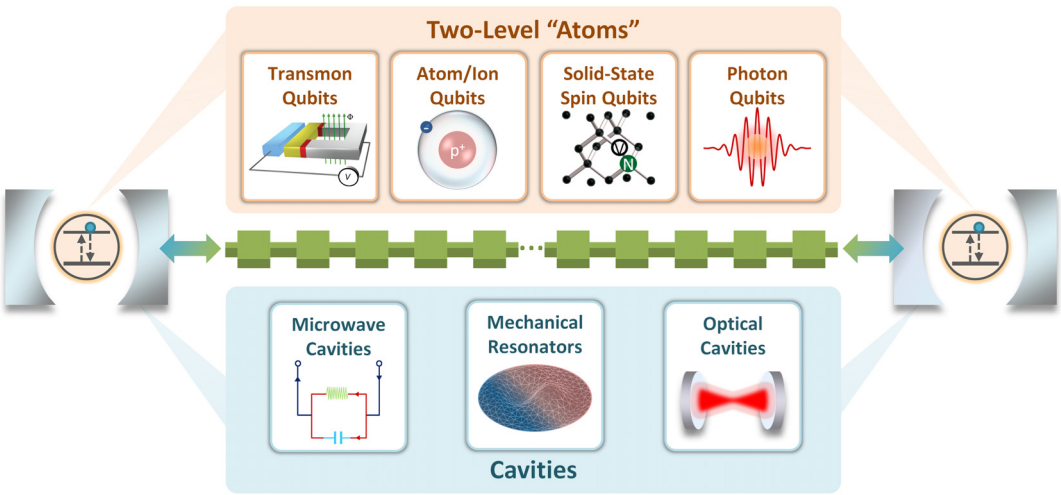

FIG. 8. Phononic waveguide bridges the coherent energy transfer and signal transduction between disparate quantum entities.

with the resonance frequency of ω_c, annihilation (a) and creation ($a^\dagger$) operators. The second term represents the energy of the qubit with the transition frequency of ω_q, lowering (σ_-) and raising (σ_+) operators. The third term represents the coupling between the cavity and emitter with the coupling strength of g. Conveniently, we assume the local cavities are high-Q mechanical resonators operating at GHz. As shown in Table II, coupling strength g in the range of 0.1–100 MHz and cooperativity C of 10–400 have been experimentally demonstrated or theoretically predicted for some key solid-state qubits.[122] When the cavity mode resonates with the transition frequency of the qubit ($\omega_q \approx \omega_c$), strong coupling allows a controlled mapping of the qubit state onto a coherent phonon superposition, which can then be mapped to an itinerant phonon in the waveguide. Moreover, traveling at significantly slower speeds than the luminal speed of photons, phonons have been suggested as better carriers, allowing quantum information to be stored, filtered, and delayed over comparatively small length scales but with high fidelity.[39,50,68]

CONCLUSIONS AND OUTLOOK

The Perspectives herein have been focused upon phononic waveguides, a family of technologically important devices that are designed to manipulate mechanical oscillations and to support the propagation of acoustic waves operating at radio to microwave frequencies. Waveguiding mechanisms and structural designs have been systematically reviewed and analyzed via numerical simulations. Mechanical properties of conventional semiconductors (*e.g.*, Si and AlGaAs), wide-bandgap materials (*e.g.*, diamond and SiC), piezoelectric materials (*e.g.*, AlN, GaN, and $LiNbO_3$), and emerging van der Waals materials (*e.g.*, graphene, TMDCs, and h-BN) have been summarized and compared for different waveguide designs. Various excitation and detection schemes have also been discussed. Moreover, based on the preliminary experimental demonstrations, the potential applications for on-chip signal transduction in both classical and quantum domains have been proposed. These Perspectives provide guidelines valuable for future designs and demonstrations of integrated phononic circuits and hybrid systems.

ACKNOWLEDGMENTS

The authors are thankful for the support from the National Science Foundation (NSF) via EFRI ACQUIRE program (Grant No. EFMA-1641099) and its supplemental funding through the Research Experience and Mentoring (REM) program, the NSF IUSE EHR program (Grant No. DUE-2142552), the NSF QuSeC-TAQS program (Grant No. OSI-2326528), the NSF EPSCoR Cooperative Agreement OIA-2044049, Nebraska's EQUATE collaboration, and the Nebraska Public Power District (NPPD) through the Nebraska Center for Energy Sciences Research (NCESR) at the University of Nebraska-Lincoln.

AUTHOR DECLARATIONS

Conflict of Interest

The authors have no conflicts to disclose.

Author Contributions

Yanan Wang: Conceptualization (equal); Data curation (lead); Formal analysis (lead); Funding acquisition (equal); Investigation (lead); Methodology (equal); Writing – original draft (lead); Writing – review & editing (equal). **Jaesung Lee:** Conceptualization (equal); Data curation (equal); Formal analysis (equal); Funding acquisition (supporting); Investigation (equal); Methodology (equal); Writing – original draft (equal); Writing – review & editing (equal). **Philip Feng:** Conceptualization (equal); Data curation (supporting); Formal analysis (supporting); Funding acquisition (lead); Investigation (supporting); Methodology (equal); Project administration (lead); Resources (lead); Supervision (lead); Writing – original draft (equal); Writing – review & editing (equal).

DATA AVAILABILITY

The data that support the findings of this study are available from the corresponding authors upon reasonable request.

REFERENCES

[1]J. Frenkel, *Wave Mechanics: Elementary Theory* (Clarendon Press, 1932).
[2]M. Maldovan, "Sound and heat revolutions in phononics," Nature **503**, 209–217 (2013).
[3]J. P. Mutschlecner and W. W. Rodney, "Infrasound from earthquakes," J. Geophys. Res. **110**, D01108, https://doi.org/10.1029/2004JD005067 (2005).
[4]A. Elfes, "Sonar-based real-world mapping and navigation," IEEE J. Rob. Autom. **3**, 249–265 (1987).
[5]S. E. Kishore, R. Sujithra, and B. Dhatreyi, "A review on latest acoustic noise mitigation materials," Mater. Today: Proc. **47**, 4700–4707 (2021).
[6]P. N. T. Wells, "Ultrasound imaging," Phys. Med. Biol. **51**, R83 (2006).
[7]M. Sledzinska, B. Graczykowski, J. Maire, E. Chavez-Angel, C. M. Sotomayor-Torres, and F. Alzina, "2D phononic crystals: Progress and prospects in hypersound and thermal transport engineering," Adv. Funct. Mater. **30**, 1904434 (2020).
[8]K. C. Kao and G. A. Hockham, "Dielectric-fibre surface waveguides for optical frequencies," in Proc. Inst. Electr. Eng. **113**, 1151–1158 (1966).
[9]E. A. J. Marcatili, "Dielectric rectangular waveguide and directional coupler for integrated optics," Bell Syst. Tech. J. **48**, 2071–2102 (1969).
[10]K. Okamoto, *Fundamentals of Optical Waveguides* (Elsevier, 2021).
[11]B. A. Auld, *Acoustic Fields and Waves in Solids* (Wiley, 1973), Vols. I and II.
[12]A. D. Pierce, *Acoustics: An Introduction to its Physical Principles and Applications* (Springer, 2019).
[13]Y. Liu, N. Dostart, and M. A. Popović, "Toward microphononic circuits on chip: An evaluation of components based on high-contrast evanescent confinement of acoustic waves," arXiv:1707.06280 (2017).
[14]V. Laude, "Principles and properties of phononic crystal waveguides," APL Mater. **9**, 080701 (2021).
[15]See https://www.engineeringtoolbox.com/air-properties-d_156.html for the Engineering ToolBox.
[16]D. R. Lide, *CRC Handbook of Chemistry and Physics* (CRC Press, 2004).
[17]R. Van Laer, B. Kuyken, D. Van Thourhout, and R. Baets, "Interaction between light and highly confined hypersound in a silicon photonic nanowire," Nat. Photonics **9**, 199–203 (2015).
[18]H. Tian, J. Liu, B. Dong, J. C. Skehan, M. Zervas, T. J. Kippenberg, and S. A. Bhave, "Hybrid integrated photonics using bulk acoustic resonators," Nat. Commun. **11**, 3073 (2020).
[19]V. T. Rathod, "A review of acoustic impedance matching techniques for piezoelectric sensors and transducers," Sensors **20**, 4051 (2020).
[20]D. J. Wilson, C. A. Regal, S. B. Papp, and H. J. Kimble, "Cavity optomechanics with stoichiometric SiN films," Phys. Rev. Lett. **103**, 207204 (2009).
[21]M. A. Fraga, H. Furlan, R. S. Pessoa, and M. Massi, "Wide bandgap semiconductor thin films for piezoelectric and piezoresistive MEMS sensors applied at high temperatures: An overview," Microsyst. Technol. **20**, 9–21 (2014).
[22]D. Mandal and S. Banerjee, "Surface acoustic wave (SAW) sensors: Physics, materials, and applications," Sensors **22**, 820 (2022).
[23]Z. Luo, A. Zhang, W. Huang, S. Shao, Y. Liu, T. Wu, and Y. Zou, "Aluminum nitride thin film based reconfigurable integrated photonic devices," IEEE J. Sel. Top. Quantum Electron. **29**, 9300119 (2023).

[24]R. S. Weis and T. K. Gaylord, "Lithium niobate: Summary of physical properties and crystal structure," Appl. Phys. A **37**, 191–203 (1985).
[25]R. Tarumi, T. Matsuhisa, and Y. Shibutani, "Low temperature elastic constants and piezoelectric coefficients of $LiNbO_3$ and $LiTaO_3$: Resonant ultrasound spectroscopy measurement and lattice dynamics analysis," Jpn. J. Appl. Phys., Part 1 **51**, 07GA02 (2012).
[26]J. E. Field, "The mechanical and strength properties of diamond," Rep. Prog. Phys. **75**, 126505 (2012).
[27]A. Falin, Q. Cai, E. J. G. Santos, D. Scullion, D. Qian, R. Zhang, Z. Yang, S. Huang, K. Watanabe, T. Taniguchi, M. R. Barnett, Y. Chen, R. S. Ruoff, and L. H. Li, "Mechanical properties of atomically thin boron nitride and the role of interlayer interactions," Nat. Commun. **8**, 15815 (2017).
[28]P. X.-L. Feng, "Resonant nanoelectromechanical systems (NEMS): Progress and emerging frontiers," in *Proceedings of IEEE 33rd International Conference on Micro Electro Mechanical Systems (MEMS)*, Vancouver, BC, Canada, 18–22 January (IEEE, 2020), pp. 212–217.
[29]F. Ye, Q. Liu, B. Xu, P. X.-L. Feng, and X. Zhang, "Ultra-high interfacial thermal conductance via double hBN encapsulation for efficient thermal management of 2D electronics," Small **19**, 2205726 (2023).
[30]B. Peng, H. Zhang, H. Shao, Y. Xu, X. Zhang, and H. Zhu, "Thermal conductivity of monolayer MoS_2, $MoSe_2$, and WS_2: Interplay of mass effect, interatomic bonding and anharmonicity," RSC Adv. **6**, 5767–5773 (2016).
[31]H. Zhu, Y. Wang, J. Xiao, M. Liu, S. Xiong, Z. J. Wong, Z. Ye, Y. Ye, X. Yin, and X. Zhang, "Observation of piezoelectricity in free-standing monolayer MoS_2," Nat. Nanotechnol. **10**, 151–155 (2015).
[32]D. Royer and E. Dieulesaint, *Elastic Waves in Solids I & II* (Springer-Verlag, 2000).
[33]L. Rayleigh, "On waves propagated along the plane surface of an elastic solid," Proc. London Math. Soc. **s1–s17**, 4–11 (1885).
[34]E. Ash, R. M. D. L. Rue, and R. F. Humphryes, "Microsound surface waveguides," IEEE Trans. Microwave Theory Tech. **17**, 882–892 (1969).
[35]A. A. Oliner, "Waveguides for acoustic surface waves: A review," in Proc. IEEE **64**, 615–627 (1976).
[36]H. Shin, W. Qiu, R. Jarecki, J. Cox, R. Olsson, A. Starbuck, Z. Wang, and P. Rakich, "Tailorable stimulated Brillouin scattering in nanoscale silicon waveguides," Nat. Commun. **4**, 1944 (2013).
[37]C. J. Sarabalis, Y. D. Dahmani, R. N. Patel, J. T. Hill, and A. H. Safavi-Naeini, "Release-free silicon-on-insulator cavity optomechanics," Optica **4**, 1147–1150 (2017).
[38]C. J. Sarabalis, J. T. Hill, and A. H. Safavi-Naeini, "Guided acoustic and optical waves in silicon-on-insulator for Brillouin scattering and optomechanics," APL Photonics **1**, 071301 (2016).
[39]W. Fu, Z. Shen, Y. Xu, C.-L. Zou, R. Cheng, X. Han, and H. X. Tang, "Phononic integrated circuitry and spin-orbit interaction of phonons," Nat. Commun. **10**, 2743 (2019).
[40]X. Zhao, L. Colombo, and C. Cassella, "Aluminum nitride two-dimensional-resonant-rods," Appl. Phys. Lett. **116**, 143504 (2020).
[41]C. Kittel, *Introduction to Solid State Physics* (John Wiley, 2005).
[42]S. Nemat-Nasser and M. Hori, *Micromechanics: Overall Properties of Heterogeneous Materials* (North-Holland, 1993).
[43]C. Mei, J. Auriault, and C. Ng, "Some applications of the homogenization theory," Adv. Appl. Mech. **32**, 277–348 (1996).
[44]A. H. Safavi-Naeini and O. Painter, "Design of optomechanical cavities and waveguides on a simultaneous bandgap phononic-photonic crystal slab," Opt. Express **18**, 14926–14943 (2010).
[45]M. Eichenfield, J. Chan, R. M. Camacho, K. J. Vahala, and O. Painter, "Optomechanical crystals," Nature **462**, 78–82 (2009).
[46]J. Gomis-Bresco, D. Navarro-Urrios, M. Oudich, S. El-Jallal, A. Griol, D. Puerto, E. Chavez, Y. Pennec, B. Djafari-Rouhani, F. Alzina, and A. Martínez, "A one-dimensional optomechanical crystal with a complete phononic band gap," Nat. Commun. **5**, 4452 (2014).
[47]K. C. Balram, M. I. Davanço, J. D. Song, and K. Srinivasan, "Coherent coupling between radiofrequency, optical and acoustic waves in piezo-optomechanical circuits," Nat. Photonics **10**, 346–352 (2016).
[48]K. Fang, M. H. Matheny, X. Luan, and O. Painter, "Optical transduction and routing of microwave phonons in cavity-optomechanical circuits," Nat. Photonics **10**, 489–496 (2016).
[49]G. S. MacCabe, H. Ren, J. Luo, J. D. Cohen, H. Zhou, A. Sipahigil, M. Mirhosseini, and O. Painter, "Nano-acoustic resonator with ultralong phonon lifetime," Science **370**, 840–843 (2020).
[50]A. Zivari, R. Stockill, N. Fiaschi, and S. Gröblacher, "Non-classical mechanical states guided in a phononic waveguide," Nat. Phys. **18**, 789–793 (2022).
[51]C. Lee, X. Wei, J. W. Kysar, and J. Hone, "Measurement of the elastic properties and intrinsic strength of monolayer graphene," Science **321**, 385 (2008).
[52]L. Song, L. Ci, H. Lu, P. B. Sorokin, C. Jin, J. Ni, A. G. Kvashnin, D. G. Kvashnin, J. Lou, B. I. Yakobson, and P. M. Ajayan, "Large scale growth and characterization of atomic hexagonal boron nitride layers," Nano Lett. **10**, 3209−−3215 (2010).
[53]C. Chen, S. Rosenblatt, K. I. Bolotin, W. Kalb, P. Kim, I. Kymissis, H. L. Stormer, T. F. Heinz, and J. Hone, "Performance of monolayer graphene nanomechanical resonators with electrical readout," Nat. Nanotechnol. **4**, 861–867 (2009).
[54]J. Lee, Z. Wang, K. He, J. Shan, and P. X.-L. Feng, "Electrically tunable single- and few-layer MoS2 nanoelectromechanical systems with broad dynamic range," Sci. Adv. **4**, eaao6653 (2018).
[55]F. Ye, A. Islam, T. Zhang, and P. X.-L. Feng, "Ultrawide frequency tuning of atomic layer van der Waals heterostructure electromechanical resonators," Nano Lett. **21**, 5508–5515 (2021).
[56]D. Hatanaka, A. Bachtold, and H. Yamaguchi, "Electrostatically induced phononic crystal," Phys. Rev. Appl. **11**, 024024 (2019).
[57]J. N. Kirchhof, K. Weinel, S. Heeg, V. Deinhart, S. Kovalchuk, K. Höflich, and K. I. Bolotin, "Tunable graphene phononic crystal," Nano Lett. **21**, 2174–2182 (2021).
[58]Q.-H. Zhang, Y. Ying, Z.-Z. Zhang, Z.-J. Su, H. Ma, G.-Q. Qin, X.-X. Song, and G.-P. Guo, "Graphene-based nanoelectromechanical periodic array with tunable frequency," Nano Lett. **21**, 8571–8578 (2021).
[59]Y. Wang, J. Lee, X.-Q. Zheng, Y. Xie, and P. X.-L. Feng, "Hexagonal boron nitride phononic crystal waveguides," ACS Photonics **6**, 3225–3232 (2019).
[60]D. Hatanaka, I. Mahboob, K. Onomitsu, and H. Yamaguchi, "Phonon waveguides for electromechanical circuits," Nat. Nanotechnol. **9**, 520–524 (2014).
[61]J. Cha and C. Daraio, "Electrical tuning of elastic wave propagation in nanomechanical lattices at MHz frequencies," Nat. Nanotechnol. **13**, 1016–1020 (2018).
[62]E. Romero, R. Kalra, N. P. Mauranyapin, C. G. Baker, C. Meng, and W. P. Bowen, "Propagation and imaging of mechanical waves in a highly stressed single-mode acoustic waveguide," Phys. Rev. Appl. **11**, 064035 (2019).
[63]S. Kim, J. Bunyan, P. F. Ferrari, A. Kanj, A. F. Vakakis, A. M. Van Der Zande, and S. Tawfick, "Buckling-mediated phase transitions in nano-electromechanical phononic waveguides," Nano Lett. **21**, 6416–6424 (2021).
[64]M. M. Sigalas, "Elastic and acoustic wave band structure," J. Sound Vib. **158**, 377–382 (1992).
[65]M. S. Kushwaha, P. Halevi, L. Dobrzynski, and B. Djafari-Rouhani, "Acoustic band structure of periodic elastic composites," Phys. Rev. Lett. **71**, 2022 (1993).
[66]R. H. Olsson and I. El-Kady, "Microfabricated phononic crystal devices and applications," Meas. Sci. Technol. **20**, 012002 (2008).
[67]A. Khelif, A. Choujaa, S. Benchabane, B. Djafari-Rouhani, and V. Laude, "Guiding and bending of acoustic waves in highly confined phononic crystal waveguides," Appl. Phys. Lett. **84**, 4400–4402 (2004).
[68]H. Shin, J. A. Cox, R. Jarecki, A. Starbuck, Z. Wang, and P. T. Rakich, "Control of coherent information via on-chip photonic–phononic emitter–receivers," Nat. Commun. **6**, 6427 (2015).
[69]B. M. Ghasemi, C. M. Reinke, B. A. Griffin, I. El-Kady, and Z. C. Leseman, "Acoustic waveguiding in a silicon carbide phononic crystals at microwave frequencies," Appl. Phys. Lett. **112**, 103504 (2018).
[70]R. N. Patel, Z. Wang, W. Jiang, C. J. Sarabalis, J. T. Hill, and A. H. Safavi-Naeini, "Single-mode phononic wire," Phys. Rev. Lett. **121**, 040501 (2018).
[71]A. Khelif, B. Djafari-Rouhani, J. O. Vasseur, P. A. Deymier, P. Lambin, and L. Dobrzynski, "Transmittivity through straight and stublike waveguides in a two-dimensional phononic crystal," Phys. Rev. B **65**, 174308 (2002).
[72]A. Khelif, Abdelkrim, A. Choujaa, B. Djafari-Rouhani, M. Wilm, S. Ballandras, and V. Laude, "Trapping and guiding of acoustic waves by defect modes in a full-band-gap ultrasonic crystal," Phys. Rev. B **68**, 214301 (2003).
[73]Y.-F. Wang, T.-T. Wang, J.-W. Liang, Y.-S. Wang, and V. Laude, "Channeled spectrum in the transmission of phononic crystal waveguides," J. Sound Vib. **437**, 410–421 (2018).

[74]Z. Yang, F. Gao, X. Shi, X. Lin, Z. Gao, Y. Chong, and B. Zhang, "Topological acoustics," Phys. Rev. Lett. **114**, 114301 (2015).
[75]R. Fleury, A. B. Khanikaev, and A. Alù, "Floquet topological insulators for sound," Nat. Commun. **7**, 11744 (2016).
[76]J. Cha, K. W. Kim, and C. Daraio, "Experimental realization of on-chip topological nanoelectromechanical metamaterials," Nature **564**, 229–233 (2018).
[77]G. Ma, M. Xiao, and C. T. Chan, "Topological phases in acoustic and mechanical systems," Nat. Rev. Phys. **1**, 281–294 (2019).
[78]A. Alù, C. Daraio, P. A. Deymier, and M. Ruzzene, "Topological acoustics," Acoust. Today **17**, 13–21 (2021).
[79]D. J. Thouless, M. Kohmoto, M. P. Nightingale, and M. den Nijs, "Quantized Hall conductance in a two-dimensional periodic potential," Phys. Rev. Lett. **49**, 405 (1982).
[80]F. D. M. Haldane, "Model for a quantum Hall effect without Landau levels: Condensed-matter realization of the 'parity anomaly'," Phys. Rev. Lett. **61**, 2015 (1988).
[81]R. Fleury, D. L. Sounas, C. F. Sieck, M. R. Haberman, and A. Alù, "Sound isolation and giant linear nonreciprocity in a compact acoustic circulator," Science **343**, 516–519 (2014).
[82]M. Xiao, G. Ma, Z. Yang, P. Sheng, Z. Q. Zhang, and C. T. Chan, "Geometric phase and band inversion in periodic acoustic systems," Nat. Phys. **11**, 240–244 (2015).
[83]X. Ni, M. Weiner, A. Alù, and A. B. Khanikaev, "Observation of higher-order topological acoustic states protected by generalized chiral symmetry," Nat. Mater. **18**, 113–120 (2018).
[84]G. Trainiti, Y. Xia, J. Marconi, G. Cazzulani, A. Erturk, and M. Ruzzene, "Time-periodic stiffness modulation in elastic metamaterials for selective wave filtering: Theory and experiment," Phys. Rev. Lett. **122**, 124301 (2019).
[85]A. Darabi, X. Ni, M. Leamy, and A. Alù, "Reconfigurable Floquet elastodynamic topological insulator based on synthetic angular momentum bias," Sci. Adv. **6**, eaba8656 (2020).
[86]N. Boechler, G. Theocharis, and C. Daraio, "Bifurcation-based acoustic switching and rectification," Nat. Mater. **10**, 665–668 (2011).
[87]R. Tabrizian, M. Rais-Zadeh, and F. Ayazi, "Effect of phonon interactions on limiting the f.Q product of micromechanical resonators," in *International Solid-State Sensors, Actuators and Microsystems Conference (TRANSDUCERS)*, Denver, CO, June 21–23 (IEEE, 2009), pp. 2131–2134.
[88]J. Rodriguez, S. A. Chandorkar, C. A. Watson, G. M. Glaze, C. H. Ahn, E. J. Ng, Y. Yang, and T. W. Kenny, "Direct detection of Akhiezer damping in a silicon MEMS resonator," Sci. Rep. **9**, 2244 (2019).
[89]L. Hackett, M. Miller, F. Brimigion, D. Dominguez, G. Peake, A. Tauke-Pedretti, S. Arterburn, T. A. Friedmann, and M. Eichenfield, "Towards single-chip radiofrequency signal processing via acoustoelectric electron-phonon interactions," Nat. Commun. **12**, 2769 (2021).
[90]V. J. Gokhale and M. Rais-Zadeh, "Phonon-electron interactions in piezoelectric semiconductor bulk acoustic wave resonators," Sci. Rep. **4**, 5617 (2014).
[91]F. Hakim, M. Ramezani, S. Rassay, and R. Tabrizian, "Non-reciprocal acoustoelectric amplification in germanium-based lamb wave delay lines," in *Proceedings of the 2019 IEEE Electron Devices Meeting (IEDM)*, San Francisco, CA, USA, December 7–11 (IEEE, 2019), pp. 198–201.
[92]L. Hackett, M. Miller, S. Weatherred, S. Arterburn, M. J. Storey, G. Peake, D. Dominguez, P. S. Finnegan, T. A. Friedmann, and M. Eichenfield, "Non-reciprocal acoustoelectric microwave amplifiers with net gain and low noise in continuous operation," Nat. Electron. **6**, 76–85 (2023).
[93]H. Mansoorzare and R. Abdolvand, "A thin-film piezo-silicon acoustoelectric isolator with more than 30 dB non-reciprocal transmission," in *Proceedings of the 2021 IEEE International Conference on Micro Electro Mechanical Systems (MEMS), Online Meeting*, January 25–29 (IEEE, 2021), pp. 470–473.
[94]C. T.-C. Nguyen, "Mechanical radio," IEEE Spectrum **46**(12), 30–35 (2009).
[95]G. K. Fedder, "CMOS-MEMS resonant mixer-filters," in *Proceeding of the 2005 IEEE International Electron Devices Meeting (IEDM)*, Washington, DC, USA, December 5 (IEEE, 2005), pp. 274–277.
[96]Y. Nakamura, Y. A. Pashkin, and J. S. Tsai, "Coherent control of macroscopic quantum states in a single-Cooper-pair box," Nature **398**, 786–788 (1999).
[97]F. Arute, K. Arya, R. Babbush, D. Bacon, J. C. Bardin, R. Barends, R. Biswas, S. Boixo, F. G. S. L. Brandao, D. A. Buell, B. Burkett, Y. Chen, Z. Chen, B. Chiaro, R. Collins, W. Courtney, A. Dunsworth, E. Farhi, B. Foxen, A. Fowler, C. Gidney, M. Giustina, R. Graff, K. Guerin, S. Habegger, M. P. Harrigan, M. J. Hartmann, A. Ho, M. Hoffmann, T. Huang, T. S. Humble, S. V. Isakov, E. Jeffrey, Z. Jiang, D. Kafri, K. Kechedzhi, J. Kelly, P. V. Klimov, S. Knysh, A. Korotkov, F. Kostritsa, D. Landhuis, M. Lindmark, E. Lucero, D. Lyakh, S. Mandrà, J. R. McClean, M. McEwen, A. Megrant, X. Mi, K. Michielsen, M. Mohseni, J. Mutus, O. Naaman, M. Neeley, C. Neill, M. Y. Niu, E. Ostby, A. Petukhov, J. C. Platt, C. Quintana, E. G. Rieffel, P. Roushan, N. C. Rubin, D. Sank, K. J. Satzinger, V. Smelyanskiy, K. J. Sung, M. D. Trevithick, A. Vainsencher, B. Villalonga, T. White, Z. J. Yao, P. Yeh, A. Zalcman, H. Neven, and J. M. Martinis, "Quantum supremacy using a programmable superconducting processor," Nature **574**, 505–510 (2019).
[98]B. E. Kane, "A silicon-based nuclear spin quantum computer," Nature **393**, 133–137 (1998).
[99]M. F. Gonzalez-Zalba, S. de Franceschi, E. Charbon, T. Meunier, M. Vinet, and A. S. Dzurak, "Scaling silicon-based quantum computing using CMOS technology," Nat. Electron. **4**, 872–884 (2021).
[100]A. Gruber, A. Dräbenstedt, C. Tietz, L. Fleury, J. Wrachtrup, and C. von Borczyskowski, "Scanning confocal optical microscopy and magnetic resonance on single defect centers," Science **276**, 2012–2014 (1997).
[101]W. Pfaff, B. J. Hensen, H. Bernien, S. B. van Dam, M. S. Blok, T. H. Taminiau, M. J. Tiggelman, R. N. Schouten, M. Markham, D. J. Twitchen, and R. Hanson, "Unconditional quantum teleportation between distant solid-state quantum bits," Science **345**, 532–535 (2014).
[102]P. C. Maurer, G. Kucsko, C. Latta, L. Jiang, N. Y. Yao, S. D. Bennett, F. Pastawski, D. Hunger, N. Chisholm, M. Markham, and D. J. Twitchen, "Room-temperature quantum bit memory exceeding one second," Science **336**, 1283–1286 (2012).
[103]M. V. G. Dutt, L. Childress, L. Jiang, E. Togan, J. Maze, F. Jelezko, A. S. Zibrov, P. R. Hemmer, and M. D. Lukin, "Quantum register based on individual electronic and nuclear spin qubits in diamond," Science **316**, 1312–1316 (2007).
[104]N. Gisin and R. Thew, "Quantum communication," Nat. Photonics **1**, 165–171 (2007).
[105]M. D. LaHaye, J. Suh, P. M. Echternach, K. C. Schwab, and M. L. Roukes, "Nanomechanical measurements of a superconducting qubit," Nature **459**, 960–964 (2009).
[106]A. D. O'Connell, M. Hofheinz, M. Ansmann, R. C. Bialczak, M. Lenander, E. Lucero, M. Neeley, D. Sank, H. Wang, M. Weides, and J. Wenner, "Quantum ground state and single-phonon control of a mechanical resonator," Nature **464**, 697–703 (2010).
[107]J.-M. Pirkkalainen, S. U. Cho, J. Li, G. S. Paraoanu, P. J. Hakonen, and M. A. Sillanpää, "Hybrid circuit cavity quantum electrodynamics with a micromechanical resonator," Nature **494**, 211–215 (2013).
[108]S. Etaki, M. Poot, I. Mahboob, K. Onomitsu, H. Yamaguchi, and H. S. J. Van der Zant, "Motion detection of a micromechanical resonator embedded in a DC SQUID," Nat. Phys. **4**, 785–788 (2008).
[109]Y. Chu, P. Kharel, W. H. Renninger, L. D. Burkhart, L. Frunzio, P. T. Rakich, and R. J. Schoelkopf, "Quantum acoustics with superconducting qubits," Science **358**, 199–202 (2017).
[110]E. A. Wollack, A. Y. Cleland, R. G. Gruenke, Z. Wang, P. Arrangoiz-Arriola, and A. H. Safavi-Naeini, "Quantum state preparation and tomography of entangled mechanical resonators," Nature **604**, 463–467 (2022).
[111]O. Arcizet, V. Jacques, A. Siria, P. Poncharal, P. Vincent, and S. Seidelin, "A single nitrogen-vacancy defect coupled to a nanomechanical oscillator," Nat. Phys. **7**, 879–883 (2011).
[112]I. Yeo, P.-L. de Assis, A. Gloppe, E. Dupont-Ferrier, P. Verlot, N. S. Malik, E. Dupuy, J. Claudon, J. M. Gérard, A. Auffèves, and G. Nogues, "Strain-mediated coupling in a quantum dot–mechanical oscillator hybrid system," Nat. Nanotechnol. **9**, 106–110 (2014).
[113]M. Montinaro, G. Wüst, M. Munsch, Y. Fontana, E. Russo-Averchi, M. Heiss, A. Fontcuberta i Morral, R. J. Warburton, and M. Poggio, "Quantum dot opto-mechanics in a fully self-assembled nanowire," Nano Lett. **14**, 4454–4460 (2014).
[114]S. Kolkowitz, A. C. Bleszynski Jayich, Q. P. Unterreithmeier, S. D. Bennett, P. Rabl, J. G. E. Harris, and M. D. Lukin, "Coherent sensing of a mechanical resonator with a single-spin qubit," Science **335**, 1603–1606 (2012).

[115]S. Hong, M. S. Grinolds, P. Maletinsky, R. L. Walsworth, M. D. Lukin, and A. Yacoby, "Coherent mechanical control of a single electronic spin," Nano Lett. **12**, 3920–3924 (2012).
[116]P. Ovartchaiyapong, K. W. Lee, B. A. Myers, and A. C. Bleszynski Jayich, "Dynamic strain-mediated coupling of a single diamond spin to a mechanical resonator," Nat. Commun. **5**, 4429 (2014).
[117]D. A. Golter, T. Oo, M. Amezcua, K. A. Stewart, and H. Wang, "Optomechanical quantum control of a nitrogen-vacancy center in diamond," Phys. Rev. Lett. **116**, 143602 (2016).
[118]M.-A. Lemonde, S. Meesala, A. Sipahigil, M. J. A. Schuetz, M. D. Lukin, M. Loncar, and P. Rabl, "Phonon networks with silicon-vacancy centers in diamond waveguides," Phys. Rev. Lett. **120**, 213603 (2018).
[119]M. Aspelmeyer, T. J. Kippenberg, and F. Marquardt, "Cavity optomechanics," Rev. Mod. Phys. **86**, 1391 (2014).
[120]M. Mirhosseini, A. Sipahigil, M. Kalaee, and O. Painter, "Superconducting qubit to optical photon transduction," Nature **588**, 599–603 (2020).
[121]W. Jiang, C. J. Sarabalis, Y. D. Dahmani, R. N. Patel, F. M. Mayor, T. P. McKenna, R. van Laer, and A. H. Safavi-Naeini, "Efficient bidirectional piezo-optomechanical transduction between microwave and optical frequency," Nat. Commun. **11**, 1166 (2020).
[122]M. J. A. Schuetz, E. M. Kessler, G. Giedke, L. M. K. Vandersypen, M. D. Lukin, and J. I. Cirac, "Universal quantum transducers based on surface acoustic waves," Phys. Rev. X **5**, 031031 (2015).